Applied Catalysis B: Environmental 90 (2009) 74–82

Contents lists available at ScienceDirect

Applied Catalysis B: Environmental

journal homepage: www.elsevier.com/locate/apcatb

Plasma-enhanced catalysis of propane and isopropyl alcohol at ambient temperature on a MnO_2-based catalyst

Julien Jarrige *, Pierre Vervisch [1]

CORIA UMR-CNRS 6614, Site universitaire du Madrillet, Avenue de l'Université, 76814 Saint–Etienne du Rouvray Cedex, France

ARTICLE INFO

Article history:
Received 16 December 2008
Received in revised form 17 February 2009
Accepted 19 February 2009
Available online 28 February 2009

Keywords:
Non-thermal plasma
MnO_2
Post-plasma treatment
VOCs removal

ABSTRACT

The removal of two volatile organic compounds (propane and isopropyl alcohol) by a nanosecond pulsed corona discharge serially combined with Al_2O_3–MnO_2 catalytic post-treatment has been investigated in air at atmospheric pressure and room temperature. The degradation mechanism of VOCs in the non-thermal plasma is a serious problem: several hazardous organic compounds (acetone and formaldehyde) are produced, and the formation yield of CO is higher than CO_2. The high concentration of ozone (up to 800 ppm) produced in the corona discharge can be used to further oxidize the VOCs on the catalyst. The efficient decomposition of O_3 on MnO_2 at ambient temperature leads to the formation of reactive oxygen species susceptible to react with residual pollutants in the effluent. This results in a significant increase of VOCs destruction and removal efficiency. Moreover, the catalytic post-treatment greatly enhances the conversion of propane into CO_2. The study of ozone-promoted decomposition mechanism of C_3H_8 on the catalyst has shown that organic by-products are adsorbed and gradually oxidized on the surface. However, concerning isopropyl alcohol, the oxidation remains incomplete: the formation yield of acetone increases after catalytic post-treatment, and the concentration of carbon oxides remains very low. The treatment of immobilized C_3H_7OH by ozone could be an alternative technique. Finally, the influence of the gas composition on the decomposition rate of ozone was also investigated.

1. Introduction

In the last 20 years, non-thermal plasma (NTP) have received great attention for environmental applications, particularly for the treatment of gas effluents containing low pollutants concentration (typically less than 1000 ppm), for which conventional industrial processes (i.e. thermal oxidation or catalytic oxidation) have a low efficiency and require high power. The treatment of gas effluents contaminated with diluted organic (VOCs) or inorganic (NO_x, SO_x) pollutants has been widely investigated with different techniques able to generate NTP, such as electron beam irradiation or electrical discharges [1].

The great advantage of these processes is the possibility to produce highly reactive species (e.g. atomic oxygen O, OH radical) in the gas at relatively low energy cost. The energy injected in the gas is indeed mainly used to generate high kinetic energy electrons, in the range 10,000–100,000 K (Te = 1–10 eV), that are not in thermal equilibrium with the heavy particles of the gas (the gas remains near room temperature). The inelastic collisions between electrons and molecules then lead to the production of active species (ions, radicals, excited species) which can react with pollutants and convert them into less hazardous compounds.

Different kinds of electrical discharges have been tested for the removal of VOCs: pulsed corona discharges [2–4], dielectric barrier discharges (DBDs) [5–7], DC corona discharges [8], surface discharges [9], photo-triggered homogeneous discharges [10], and ferroelectric packed-bed DBD [11,12]. The influence of the gas parameters has been widely investigated. It has been shown that the temperature [2,7] and the amount of O_2 and H_2O (precursors of O and OH radicals) in the gas [13,14] have a significant influence on the efficiency of the process. The destruction rate was seen to decrease when increasing the initial concentration of VOCs [2,6].

However, the nature and the concentration of the by-products associated with the degradation of VOCs are a serious problem preventing an industrial application. These last years, the combination of NTP with heterogeneous catalysis has emerged as a promising technique to improve the efficiency of VOCs removal. The combination can be operated in two configurations [15]: single-stage (also called plasma-driven catalysis PDC) where catalysts are placed in the discharge reactor, directly exposed to

* Corresponding author. Tel.: +33 232953648; fax: +33 232910485.
E-mail addresses: jjarrige@odu.edu (J. Jarrige), pierre.vervisch@coria.fr (P. Vervisch).
[1] Tel.: +33 232953612; fax: +33 232910485.

0926-3373/$ – see front matter © 2009 Elsevier B.V. All rights reserved.
doi:10.1016/j.apcatb.2009.02.015

the non-thermal plasma, and two-stage (plasma-enhanced catalysis, PEC), where catalysts are placed downstream the NTP unit.

Plasma-driven catalysis systems aim at creating synergy effects between catalytic material and electrical discharges. A Pt-based monolith catalyst was seen to be efficiently activated by a DBD discharge, leading to a complete destruction of 2-heptanone with an enhanced CO_2 selectivity [16]. Electrodes coated with catalytic material were also tested, showing an significant improvement of trichloroethylene and isopropyl alcohol destruction efficiency and higher conversion rates into CO_2 [17,18]. Using VOCs immobilized on porous alumina and silica gel, Holzer et al. [19] showed that short-lived reactive species were present inside the intra-particle volume of the material when placed the discharge zone. In an additional work, the role of ozone in the destruction mechanisms of VOCs was investigated [20]. Manganese dioxide (MnO_2) was also tested as a catalytic material inside the discharge, showing a reduction of ozone concentration and an enhancement of NTP performance [21]. Several studies focused on the combination of photocatalysts (e.g. TiO_2) with NTP [21–24]. No evidence of catalyst photo-activation by UV emissions from the discharge was seen, but some synergetic effects have been reported for the removal of benzene, acetylene, acetone and toluene.

Pre-treatment of effluents by NTP before catalytic treatment (metal oxides) showed promising results for the destruction of a wide range of VOCs [25]. A Pt-based catalyst combined with a pulsed corona reactor enabled the by-products formation to be reduced, and partly converted CO into CO_2 at 210 °C [26]. It was shown that ozone plays an important role in the mechanism. A higher activity of alumina catalyst for methane oxidation (in the temperature range 300–500 °C) was observed when combined with a DBD [27]. Synergetic effects, attributed to ozone decomposition, were found between electrical discharges and Mn-based phosphate catalysts during oxidation of toluene [28]. The serial combination of NTP and MnO_2 catalyst greatly enhanced the destruction efficiency of benzene [29], toluene [30] and trichloroethylene [31], and efficiently reduced O_3 emissions.

The aim of the present work is to study a non-thermal plasma catalysis enhanced system composed of nanosecond pulsed corona discharges and a fixed-bed MnO_2–Al_2O_3 catalytic post-treatment at ambient temperature. The degradation mechanisms of two VOCs (propane and isopropyl alcohol) are investigated both in the plasma phase and on the catalyst surface.

2. Experimental

The schematic diagram shown in Fig. 1 presents an overview of the experimental setup used in this study.

2.1. Non-thermal plasma reactor and catalyst fixed-bed

The non-thermal plasma is produced by a corona discharge in air at atmospheric pressure and ambient temperature. In typical dielectric barrier discharge configuration the distance between the electrodes is generally less than 10 mm. On the other hand, corona discharges can develop in longer gaps (several centimetres), so the volume of discharge reactor is increased. Consequently, the residence time of the polluted gas stream in the reactor is higher and larger flow rates can be decontaminated. This is more suitable for an industrial application.

The corona reactor is designed in a wire to cylinder configuration. The inner electrode is a tungsten wire with a diameter of 100 μm. The cathode is a stainless steel cylinder with an internal diameter of 56 mm. The length of the discharge zone is 570 mm and the volume of the effective plasma zone is about 1.4 L. This corresponds to a residence time of 6 s for a flow rate of 14 L/min.

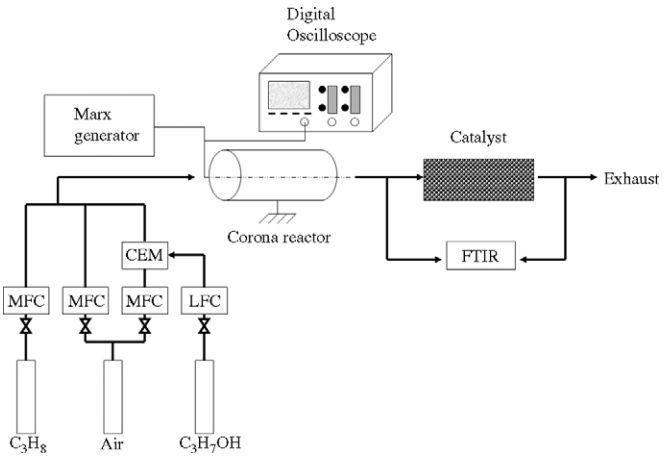

Fig. 1. Schematic diagram of the experimental setup.

The curve radius of the wire is intentionally very small in order to locally increase the reduced electric field in the vicinity of the anode. This favors the development of primary electronic avalanches and enhances the formation of the space charge. Electrical signals show that streamers can develop in the reactor when applying voltage as low as 35 kV.

A post-plasma treatment of the effluent was performed in a catalysis fixed-bed reactor. A commercial catalyst (N84, Sud-Chemie) was used. The catalyst material consists of porous alumina (γ-Al_2O_3) coated with manganese dioxide (MnO_2). The catalyst is extruded in a cylindrical shape with an average diameter of 7 mm and length of 15 mm. The volume of MnO_2-coated alumina cylinders in the experiments was varied between 60 and 400 cm^3, i.e. the gas hour space velocity (GHSV) in the catalytic reactor is between 2500 and 15,000 h^{-1}. The gas effluent was not heated before the discharge reactor or the catalyst.

2.2. High-voltage pulse forming system and electrical measurements

One of the main drawbacks of corona discharges is the streamer to spark transition that can occur once the streamers have crossed the gap. If the applied voltage remains too high after streamer-cathode junction then a very intense conduction current can circulate in the residual ionized channels. The electrons extracted from the cathode during this phase of conduction mainly dissipate their energy by heat transfer, rather than by inelastic collisions. This results in low radical production efficiency. High-voltage pulses with a short width (i.e. a few hundreds of nanoseconds) are commonly used in this kind of configuration in order to quickly reduce the voltage value.

In our experimental setup, the corona discharge was driven by a homemade two-stage Marx generator, which has been described in detail previously [32]. It uses spark gaps filled with hydrogen under pressure (10–20 bars) as commutators. The storing capacitors were 560 pF, and a 3300 Ω resistor was placed parallel to the discharge reactor in order to evacuate residual charges from one pulse to another.

This system enables the formation of positive high-voltage pulses with amplitude between 40 and 80 kV, and a 4.5 ns constant rise time. The pulse repetition rate could be varied from 1 to 1000 Hz.

Typical voltage and current waveforms of the corona reactor during a discharge in dry air are shown in Fig. 2. The current and voltage were recorded using a high voltage capacitive probe (Effitech, 1/1000 divider, 1 GHz) and a Rogowski coil (Prodyn I-125, 80 kHz–500 MHz). Current and voltage waveforms were mon-

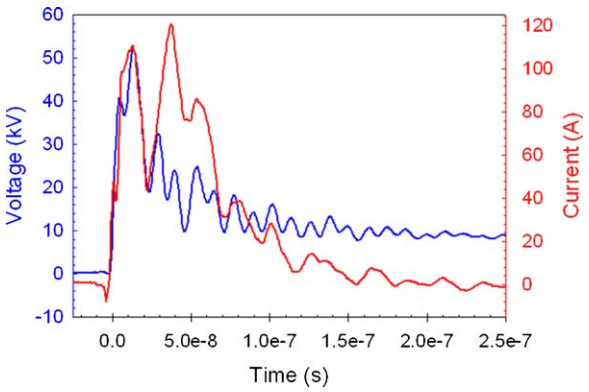

Fig. 2. Typical current and voltage waveforms across the corona discharge reactor (in dry air).

itored by a 1 GHz digital oscilloscope (Tektronix TDS 7104, 10 Gsamples/s).

The amplitude of the high-voltage pulse is 52 kV, with a very short rise time (4.5 ns). The voltage then quickly decreases below 20 kV after 60 ns and below 10 kV after 150 ns. The current waveform is composed of two main peaks: the first one during the discharge initiation (around 10 ns), and the second one after the arrival of the streamers at the cathode (around 45 ns). The current has amplitude of about 120 A, and decreases to zero after 150 ns.

The power and the energy injected in the discharge were calculated by multiplying current and voltage signals and integrating this product over the pulse width. The results are shown in Fig. 3. The power injected in the corona discharge has very high amplitude of 5.6 MW. All the energy is deposited in the plasma in a very short time (150 ns), and the total energy per pulse is about 165 mJ.

2.3. Gas-flow generation and gas composition analysis

For all experiments, contaminated gas flow rates used industrial dry air (Messer) as a carrier gas (N_2/O_2: 80/20). Gas streams of air and propane were generated from compressed gas cylinders. Their respective flow rates were regulated using mass flow controllers (Bronkhorst). Isopropyl alcohol vapor was added to the air stream using a controlled evaporating and mixing chamber (CEM) from Bronkhorst. The gas flow rate was fixed at 14 L/min for all experiments.

The gas composition was analyzed online using a Fourier transform infra-red (FTIR) absorption spectrometer Avatar 370 (Thermo Nicolet) equipped with a 2 m long multiple pass absorption cell. Spectra are acquired in the wave numbers ranging 650–4000 cm^{-1} with a resolution of 0.5 cm^{-1}. It enabled the identification and quantification of organic and inorganic compounds such as propane (C_3H_8), isopropyl alcohol (C_3H_7OH), acetone (C_3H_6O) formaldehyde (HCHO), carbon monoxide (CO), carbon dioxide (CO_2), and ozone (O_3).

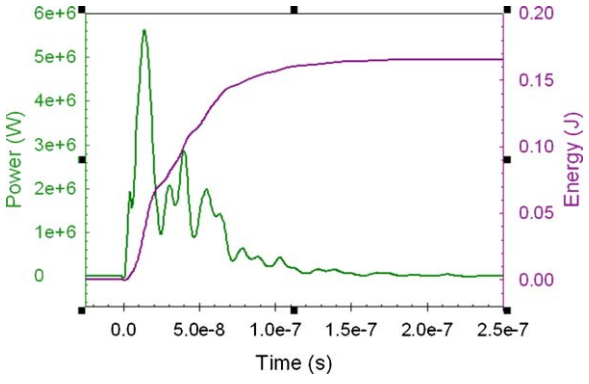

Fig. 3. Power and energy deposited in the corona discharge reactor (in dry air).

The composition of the gas at the outlet of the corona discharge reactor and downstream from the fix-bed catalyst is compared in order to determine the different degradation mechanisms in the non-thermal plasma and on the MnO_2 catalytic sites.

3. Characteristic parameters

The decomposition results are shown as a function of the specific input energy (SIE), which expresses the amount of energy deposited in the gas per unit of volume:

$$\mathrm{SIE\,(J/L)} = \frac{P}{Q} = \frac{f \times E}{Q}$$

where P is the power dissipated in the discharge (W), f the pulse repetition rate (Hz), E the energy deposited by pulse (J), and Q the gas flow rate through the corona reactor (L/s).

In the following experiments, SIE was varied by changing the pulse repetition frequency. The amplitude and the energy of HV pulse were kept constant for each series. Our previous works have shown that pulse amplitude and rise time do not influence the efficiency of the corona discharge process. They also show that the only effective parameter was the specific input energy [32].

The destruction and removal efficiency (DRE) of propane and isopropyl alcohol is expressed as:

$$\mathrm{DRE\,(\%)} = 100 \times \left(\frac{[X]_{\mathrm{in}} - [X]_{\mathrm{out}}}{X_{\mathrm{in}}}\right)$$

where $[X]_{\mathrm{in}}$ and $[X]_{\mathrm{out}}$ (ppm) are the concentrations of pollutants at the inlet and the outlet of the chemical reactors.

The conversion of the pollutant X into a carbonaceous by-product B is evaluated using the formation yield Y_B:

$$Y_B\,(\%) = 100 \times \frac{[B] \times n_B}{([X]_{\mathrm{in}} - [X]_{\mathrm{out}}) \times n_X}$$

where $[B]$ is the concentration of the by-product, n_X and n_B are the number of carbon atoms in the pollutant and in the by-product molecule, respectively. The formation yield is a key parameter to compare the degradation pathways and to estimate the rate of oxidation of the VOC's.

4. Results

4.1. Preliminary study: decomposition of VOCs by non-thermal plasma treatment alone

4.1.1. Propane

An air stream of 1 m^3/h containing 500 ppm of propane was treated in the corona reactor. The decomposition of C_3H_8 and the formation of by-products in the discharge are shown in Fig. 4. The concentration of propane steadily decreases when SIE increases, and its minimum value is 157 ppm at 490 J/L, i.e. a DRE of 68.4%. Three by-products were quantified: formaldehyde (HCHO), carbon monoxide (CO) and carbon dioxide (CO_2). No C_2 or C_3 organic compounds (e.g. aldehydes, acids, or alcohols) were detected after NTP treatment, even for the lower SIE. Standard plasma radical kinetics based on O and OH oxidation of the compounds (with formation of organic peroxy radicals by O_2 addition) fails to explain this distribution of the by-products. Therefore the decomposition of C_3H_8 in the discharge must proceed through a fast cleavage of the C–C bonds. Several processes could be implied in the degradation mechanism: direct electronic impact and chemical reactions with ions or nitrogen excited states. Dissociation of propane could lead to the production of methyl radical CH_3, which

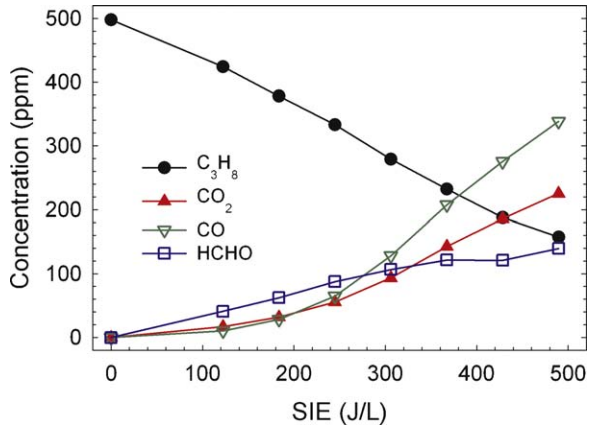

Fig. 4. Formation of by-products during the NTP treatment of propane ($[C_3H_8]_{init}$ = 500 ppm).

is an important intermediate in the formation kinetics of HCHO. A kinetic mechanism for propane degradation based on dissociation of the molecule is proposed in Fig. 5.

Formaldehyde is the main by-product for the lower specific energy (less than 300 J/L). At 184 J/L, the concentrations of HCHO, CO and CO_2 are 63, 31 and 31 ppm, respectively. When the specific energy is further increased, HCHO is eliminated by reactions with atomic oxygen. This leads to the formation of formyl radical HCO°, which mainly liberates CO and, to a less extent, CO_2:

$$HCHO + O \rightarrow HCO^\circ + HO^\circ$$

$$HCO^\circ + O_2 \rightarrow CO + HO_2{}^\circ$$

$$HCO^\circ + O \rightarrow CO + HO^\circ$$

$$HCO^\circ + O \rightarrow CO_2 + H$$

The above-mentioned reactions are responsible for the increase of CO, which becomes the major by-product over 300 J/L. For the highest SIE (490 J/L), concentrations of CO, CO_2 and HCHO are 340, 225 and 140 ppm, respectively. Carbon balance for propane is between 78% and 90% for the investigated range of specific input energies.

Another important by-product of propane, which has not been quantified, is methyl nitrate CH_3ONO_2. Strong absorbance bands were detected on FTIR spectra in the wave numbers ranging 820–880 and 1260–1320 cm^{-1} (Fig. 6). Since no significant NO_x species were measured after the discharge, the formation of this compound is still unexplained [32].

4.1.2. Isopropyl alcohol

The decomposition of isopropyl alcohol in the discharge (initial concentration: 500 ppm) shows a better efficiency than propane

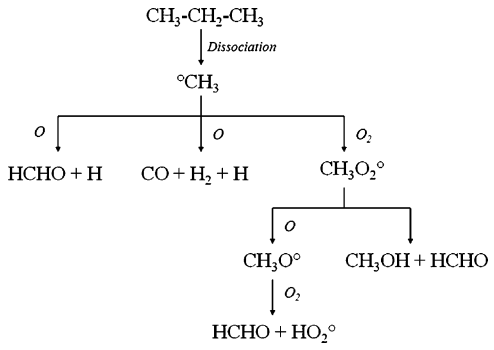

Fig. 5. Degradation mechanism of propane in the corona discharge.

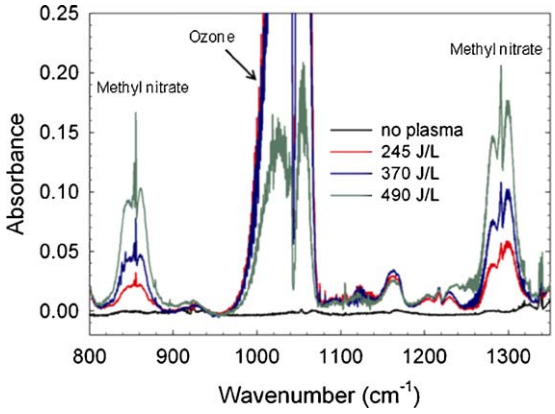

Fig. 6. Evolution of FTIR spectra of the effluent during NTP treatment of propane.

(Fig. 7). At 330 J/L, the residual concentration is only 40 ppm, i.e. a destruction efficiency of 92%. The main by-product is acetone (C_3H_6O), whose concentration increases up to 285 ppm at 248 J/L, and slightly decreases for higher specific input energies. The different behaviours of C_3H_7OH and C_3H_8 in the non-thermal plasma could be explained by their reactivity with atomic oxygen. Isopropyl alcohol is indeed more reactive with O at ambient temperature ($k = 6.64 \times 10^{-14}$ cm^3 $molecule^{-1}$ s^{-1}) than propane ($k = 8.3 \times 10^{-15}$ cm^3 $molecule^{-1}$ s^{-1}). Then oxidation of C_3H_7OH by O is more likely to happen, and dissociation processes (C–C bonds cleavage) do not dominate in the degradation mechanism.

The formation of acetone is due to oxidation of isopropyl alcohol by atomic oxygen, which leads to the dehydrogenation of the molecule:

$$CH_3CH(OH)CH_3 + O \rightarrow CH_3C^\circ(OH)CH_3 + HO^\circ$$

$$CH_3C^\circ(OH)CH_3 + O_2 \rightarrow CH_3C(O)CH_3 + HO_2{}^\circ$$

$$CH_3C^\circ(OH)CH_3 + O \rightarrow CH_3C(O)CH_3 + OH^\circ$$

The formation yield of acetone is very high, between 55% and 75%. Acetone is much less reactive with O or OH than isopropyl alcohol; therefore its decomposition in the corona discharge would require very high specific input energies (several kJ/L) at ambient temperature.

At the same time, degradation of isopropyl alcohol leads to the formation of formaldehyde. HCHO concentration increases with SIE up to 200 J/L, and then remains constant, around 100 ppm, for higher SIE, where formation rate and decomposition rate of formaldehyde are the same. HCHO represents 11–14.5% of the

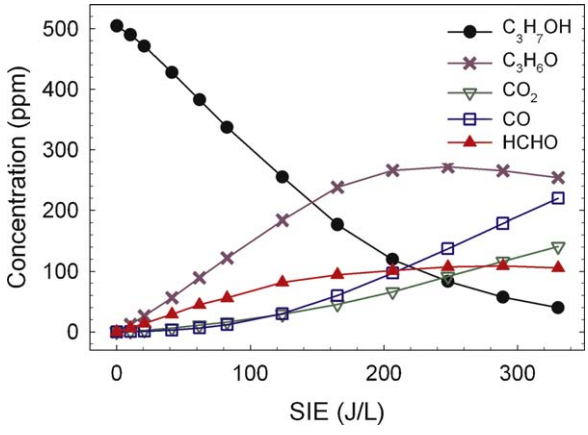

Fig. 7. Formation of by-products during NTP treatment of isopropyl alcohol ($[C_3H_7OH]_{init}$ = 500 ppm).

conversion products from 10 to 120 J/L. The production of CO and CO_2 is almost negligible (less than 5%) until HCHO begins to be significantly oxidized in the plasma. At 330 J/L, the formation yield of HCHO decreases to 7.5%, whereas the conversion rates of CO and CO_2 reach 15.8% and 10.1%. Carbon balance is higher than for propane removal (more than 85%) but not complete. Traces of methyl nitrate and formic acid have also been detected on FTIR spectra.

4.2. Limits of non-thermal plasma techniques for the depollution of gas effluents

The previous results have shown that atmospheric pressure corona discharges exhibit good performances for the gas phase removal of 500 ppm of propane and isopropyl alcohol in dry air. High DRE are obtained for input energies less than 500 J/L. However, this study has revealed that non-thermal plasma processes still have some serious limits that prevent using this promising technology on an industrial scale.

First, several hazardous organic compounds (e.g. aldehydes and ketones) are produced during the decomposition of the pollutant. Some of these molecules could be even more toxic than VOC that are removed from the effluent. For example, formaldehyde is known as a highly toxic, allergenic, and carcinogenic compound.

Second, high CO concentrations (a few hundred ppm) are obtained following corona discharge treatment, whereas gas depollution processes aim at a complete mineralization of polluting compounds, i.e. production of CO_2 and H_2O. The conversion into CO is indeed favored over CO_2 in the NTP degradation mechanisms of C_3H_8 and C_3H_7OH, as shown in Fig. 8. CO/CO_2 ratio increases with DRE for both compounds and is over 1.4 for the higher destruction rates (>60%).

Third, even though the energy cost for VOC removal is reasonable, the formation of organic by-products implies that much higher specific input energies must be injected in the discharge in order to achieve a complete detoxification of the gas stream.

Finally, huge amounts of ozone are produced in the discharge, as can be seen in Fig. 9. O_3 concentration at the outlet of the NTP reactor can reach values as high as 800 ppm. It is noticeable that higher ozone concentrations (more than 900 ppm) have been measured in pure air streams (when no VOCs were added in the gas).

The formation of O_3 in a gas discharge is a well known process, following a three-body reaction between atomic oxygen and molecular oxygen:

$$O + O_2 + M \rightarrow O_3 + M$$

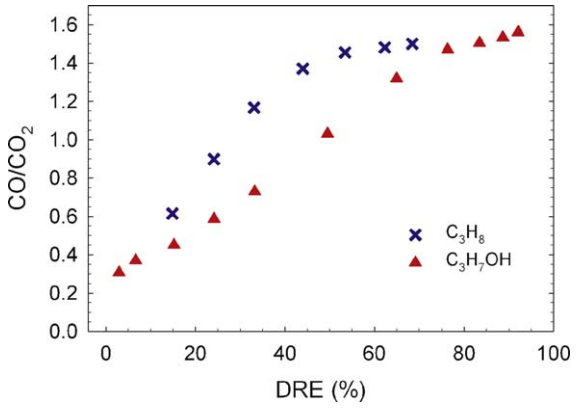

Fig. 8. Evolution of CO/CO_2 ratio during NTP treatment of propane and isopropyl alcohol.

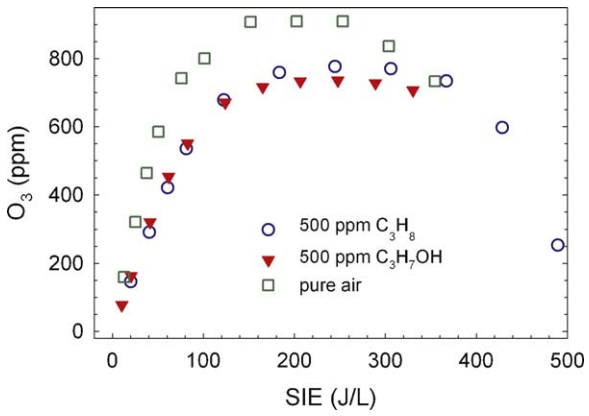

Fig. 9. Production of ozone in the corona discharge.

Ozone emissions in the atmosphere are not desirable, as O_3 is responsible for respiratory diseases and is implied in the formation of smog over big cities. Moreover, oxygen atoms that are consumed in the formation of ozone are not available for the elimination of pollutants in the effluent. Therefore, a significant part of the energy that has been injected in the discharge to create high energy electrons, which produce radicals by dissociation of molecular oxygen, is wasted in the production of ozone.

4.3. Post-plasma treatment by Al_2O_3–MnO_2 catalyst

The post-treatment reactor filled with Al_2O_3–MnO_2 cylinders is placed downstream from the NTP reactor. The residence time of the gas in the pipe between the outlet of the plasma reactor and the catalyst is around 0.1 s. The catalyst cannot be activated by the active species of the discharge (atoms, radicals, charged species, and UV photons) as in plasma-driven catalysis process, and only long-lived species can react on the catalytic sites (e.g. ozone).

MnO_2-based catalysts are well known for their ability to decompose ozone at low temperatures. Futamura [21] proposed the following degradation mechanism of VOCs for MnO_2-based catalysts:

- The decomposition of O_3 on the surface of MnO_2 leads to the production of adsorbed atomic oxygen O*.
- O* can react with pollutants on the surface (Rideal–Eley mechanism).
- O* can be desorbed, and released $O(^3P)$ atoms can react with VOCs in the gas phase.

4.4. Propane

The effect of the combination of NTP and Al_2O_3–MnO_2 catalyst on the removal of propane was investigated. Initial concentration of C_3H_8 in the gaseous effluent at the inlet of plasma-catalytic system was 200 ppm, and the volume of catalyst was fixed at 400 cm^3 for the following experiments (GHSV = 2500 h^{-1}). Ozone was almost completely decomposed on Al_2O_3–MnO_2. Residual O_3 concentration in the effluent downstream the fixed-bed reactor remains less than 5 ppm, whereas O_3 production in the corona discharge reaches 800 ppm.

Destruction and removal efficiencies and energy cost at the outlet of the corona reactor and the fixed-bed reactor are compared in Fig. 10. The performance of the NTP process was noticeably improved when catalytic post-treatment was added. At 100 J/L, DRE after plasma treatment was only 19%, whereas it reached 65% with catalytic post-treatment and at 200 J/L, DRE was doubled (from 43% to 84%). In the mean time, the energy required for the destruction of one molecule of propane was reduced by a factor up

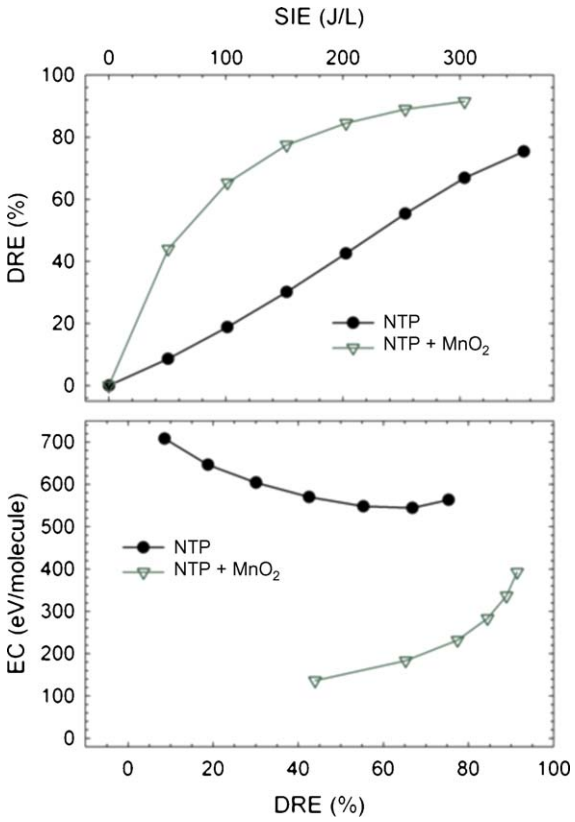

Fig. 10. Effect of Al_2O_3–MnO_2 catalyst on DRE and energy cost of propane ($[C_3H_8]_{init}$ = 200 ppm).

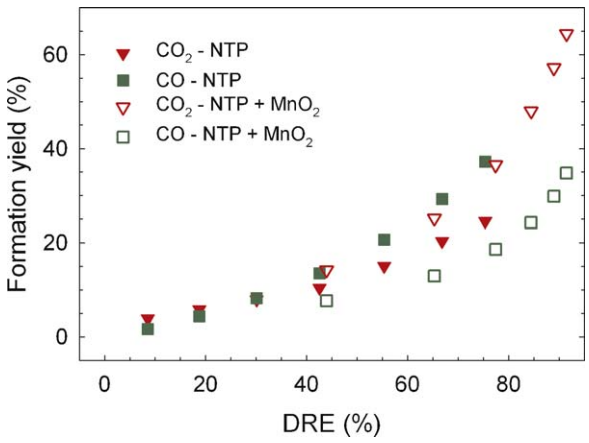

Fig. 11. Effect of Al_2O_3–MnO_2 catalyst on the formation of carbon oxide during the decomposition of propane ($[C_3H_8]_{init}$ = 200 ppm).

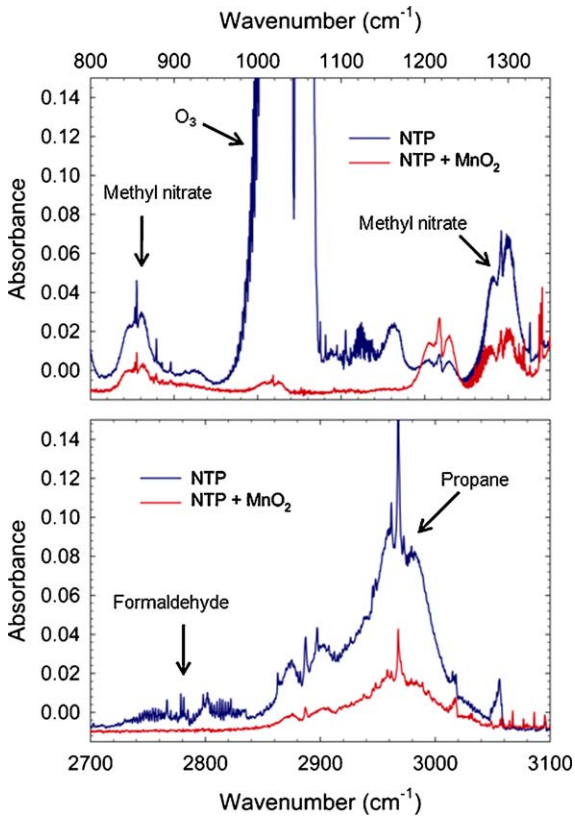

Fig. 12. Comparison of FTIR spectra after NTP treatment and after catalytic post-treatment.

to four. Energy cost of propane removal in plasma-catalytic system increases with DRE, i.e. when the specific input energy is increased. This can be explained by two main reasons. First, the production of ozone does not increase linearly with SIE deposited in the discharge, as can be seen in Fig. 9. Ozone concentration is almost constant from 200 to 300 J/L, so the energy cost for the production of oxygen atoms susceptible to react with residual C_3H_8 on MnO_2 sites increase with SIE. The fraction of propane removed in the fixed-bed reactor does not increase in this energy range, and could even be reduced. Second, residual C_3H_8 concentration after NTP treatment decreases when increasing SIE. The efficiency of VOC decomposition on the catalyst also depends on its concentration, as will be seen later in this paper.

No adsorption of propane was observed in the fixed-bed reactor. The analysis of carbon monoxide and carbon dioxide content of the gas stream (in Fig. 11) shows that chemical destruction of C_3H_8 occurs in the packed-bed reactor. CO and CO_2 concentration both significantly increase following catalytic post-treatment. Moreover, for a given destruction efficiency of propane, the selectivity of CO and CO_2 are modified under the effect of the catalyst. The formation yield of CO_2 is higher than in the case of NTP treatment alone, whereas the formation yield of CO decreases. This results in a more acceptable CO/CO_2 ratio that remains constant around 0.5, in comparison to the ratio at the outlet of electrical discharge reactor (up to 1.4).

FTIR spectra of the effluent treated by NTP and NTP-catalysis are compared in Fig. 12. Absorption signals in the wave numbers 2700–2850 cm^{-1} indicate that the formaldehyde (HCHO) that is produced during the degradation of propane in the corona discharge reactor was completely removed in the fixed-bed reactor. Furthermore, methyl nitrate (CH_3NO_3) bands are significantly reduced. However, the comparison of carbon balance reveals that a part of the organic compounds is trapped in the packed-bed reactor. At 200 J/L, carbon balance after NTP processing of the effluent is more than 78%, whereas it is below 68% after catalyst post-treatment. At this energy, 65% of initial propane has been removed. Adsorption phenomena are probably responsible for this loss of carbon.

Further experiments were performed in order to verify this assumption. Following the propane removal experiments on NTP-catalyst system, the packed-bed reactor was fed by an ozone-loaded air stream (500 ppm) which was free of carbon-containing compounds (VOCs, CO or CO_2). The temporal evolution of the gas stream composition at the outlet of the catalyst reactor was monitored using FTIR spectrometer (Fig. 13). During the first minutes of the experiment, ozone was completely removed on the

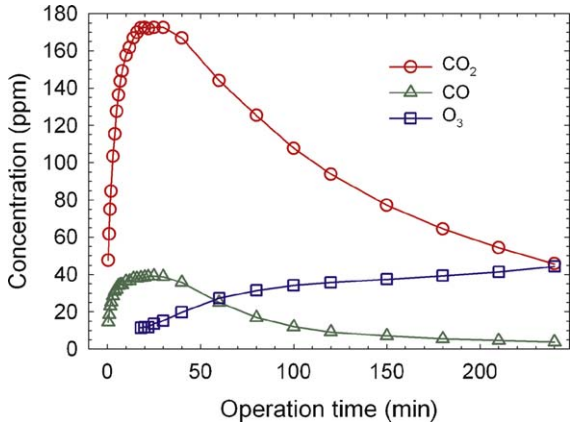

Fig. 13. Carbon oxide formation and residual ozone concentration during the cleaning of the catalyst by O_3 ($[O_3]_{inlet}$ = 500 ppm).

catalyst surface and production of carbon oxides is detected. The formation of CO and CO_2 can only be explained by the presence on the catalyst surface of immobilized organic compounds, which are oxidized by oxygen atoms produced in the decomposition process of O_3. The concentration of CO and CO_2 increases up to 25 min, with respective maximum values of 40 and 175 ppm, and then slowly decreases. After 4 h of exposition to ozone, CO and CO_2 concentrations are 4 and 46 ppm. It is noteworthy that CO/CO_2 ratio is lower than for NTP-catalysis process (between 0.08 and 0.2). In the mean time, a continuous increase in residual ozone concentration in the effluent occurs during the process. Roland et al. [20] also reported a reduction of the capability of Al_2O_3 to decompose O_3 during the treatment of immobilized VOCs in post-plasma treatment. The authors suggested that CO_2 molecules produced during degradation of organic compounds poison the catalytic sites.

The decomposition mechanism of propane on Al_2O_3–MnO_2 catalyst alone was also investigated. In this experiment, a dry air stream is passing through the corona reactor where ozone is produced. Then a known concentration of propane is injected in this ozone-enriched air stream before the inlet of the fixed-bed reactor. The chemical activity of the catalyst can then be studied without the preliminary degradation of VOC by corona discharges. The only possible destruction mechanism is the action of atomic oxygen resulting from ozone decomposition on Al_2O_3–MnO_2. The amount of removed propane as a function of initial ozone concentration is shown in Fig. 14. For all initial propane concentrations, the amount of removed C_3H_8 increases with O_3 concentration. The addition of 800 ppm of O_3 to 200 ppm of C_3H_8 in air enables the removal of 160 ppm, i.e. a decomposition efficiency of 80%. On the other hand, for a given concentration of ozone in the gas, the amount of removed C_3H_8 increases with the initial propane content. The only detected by-products on FTIR spectra were carbon dioxide and carbon monoxide. The production of CO and CO_2 during ozone-promoted-catalysis decomposition of propane is shown in Fig. 15. Even though CO_x formation increases with C_3H_8 removal rate, the concentrations remain relatively low. At initial concentration of 200 ppm, the formation yields of CO and CO_2 reach respective values of 9% and 25%. CO_x formation seems to be enhanced when decomposition rate of propane is improved. For higher initial content of C_3H_8 (500 and 1000 ppm), the formation yield are even lower (less than 5%). In all cases, CO/CO_2 ratio is less than 0.7, and they tend to decrease when propane removal rate is raised. The ozone-promoted destruction of C_3H_8 on MnO_2 leads to the formation of several organic by-products that remain adsorbed on the catalyst. Reactive oxygen species available on the surface then gradually oxidize these adsorbed compounds. Complete conversion leads to the formation of CO_2, H_2O (and to a less extent CO) which are then released in the gas phase.

Additional experiments did not show an effective conversion of CO into CO_2 on the catalyst with O_3. Therefore, the change in carbon oxides formation yield is only due to the degradation mechanism on Al_2O_3–MnO_2. The catalyst clearly favors the conversion of propane into CO_2.

4.4.1. Isopropyl alcohol

The same experimental setup was used to study the removal of isopropyl alcohol for an initial concentration of 500 ppm. As can be seen in Fig. 16, the formations of CO_2 and, to a less extent, of CO are enhanced by Al_2O_3–MnO_2 catalyst, which shows that a further

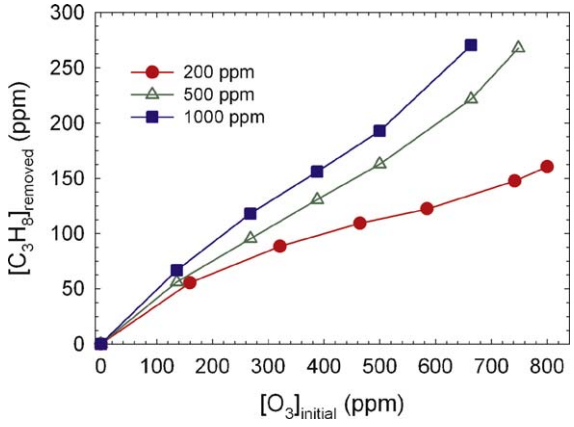

Fig. 14. Ozone-promoted decomposition of propane on Al_2O_3–MnO_2 catalyst for different initial concentrations.

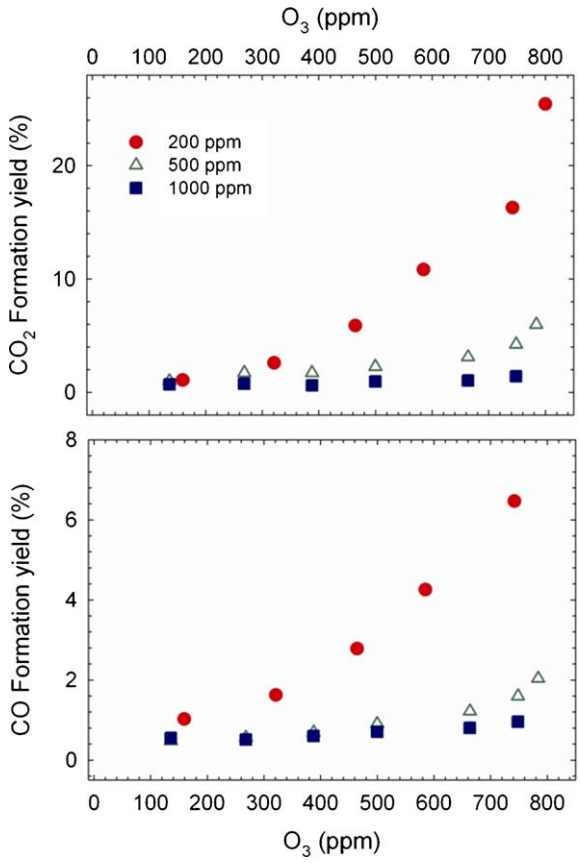

Fig. 15. Carbon oxides formation during ozone-promoted destruction of propane on Al_2O_3–MnO_2 catalyst.

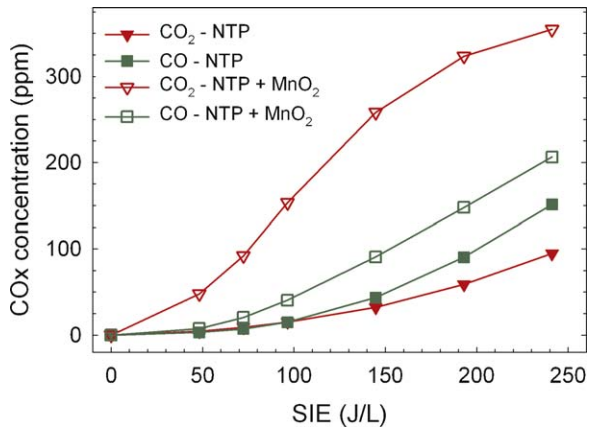

Fig. 16. Effect of Al_2O_3–MnO_2 catalyst on the formation of carbon oxide during the treatment of isopropyl alcohol ($[C_3H_7OH]_{init}$ = 500 ppm).

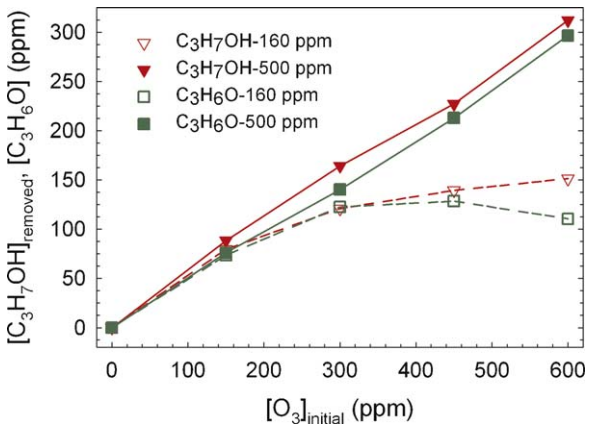

Fig. 17. Decomposition of isopropyl alcohol and formation of acetone during ozone-promoted Al_2O_3–MnO_2 catalysis for two different initial concentration (140 and 500 ppm).

oxidation is obtained. Formaldehyde is completely removed, and acetone concentration slightly diminishes. However, since C_3H_7OH is totally absorbed in the fixed-bed reactor, it was not possible to compare the DRE or to determine if the rise in CO_x production after catalytic treatment is due the degradation of isopropyl alcohol or of its organic by-products.

A second series of experiments was performed in order to understand the degradation mechanism in the fixed-bed reactor. A smaller volume of catalyst (66 cm^3, GHSV = 15,000 h^{-1}) was saturated in isopropyl alcohol beforehand. A contaminated gas stream (14 L/min) was passed through the fixed-bed reactor until the concentration of C_3H_7OH upstream and downstream was the same. Two specific input energies were studied: 48 and 96 J/L. Table 1 presents the results of the NTP-catalysis treatment on isopropyl alcohol removal. As with propane, NTP-catalysis process significantly improves the destruction efficiency of isopropyl alcohol. At 96 J/L, the residual concentration of C_3H_7OH is 265 ppm after corona discharge treatment, whereas the removal is almost complete at the outlet of the catalytic bed (60 ppm). The energy cost is reduced by a factor 3 at 48 J/L, and by a factor 2 at 96 J/L. On the other hand, acetone produced during the degradation of C_3H_7OH in the discharge is not degraded in the catalytic bed, and the concentration of C_3H_6O even increases. The formation yield of C_3H_6O is more than 80% following NTP-catalysis process. Even though the concentrations of CO and CO_2 are increased following catalytic post-treatment, their formation yield remain very low (less than 5.5%), like formaldehyde. Isopropyl alcohol seems to be mainly converted into acetone on the catalytic sites. Since the volume of the catalyst was reduced, less active sites were available for the decomposition of ozone, and residual O_3 concentration is more than 100 ppm. Because of adsorption–desorption phenomena in the fixed-bed, experiments were run for a long time (more than 1 h) in order to get stable concentrations at the outlet of the reactor. The concentration of ozone at 48 and 96 J/L remain constant during the experiment, so Al_2O_3–MnO_2 does not seem to be deactivated during the treatment. Contrary to propane removal, carbon balance is high (around 96%) after catalytic post-treatment.

Table 1
Comparison of NTP and NTP/MnO_2 treatment of isopropyl alcohol (initial concentration: 500 ppm).

	SIE (J/L)	DRE (%)	EC (eV/molecule)	Formation yield (%)			
				C_3H_6O	HCHO	CO	CO_2
NTP alone	48	22	109	54.1	12.5	1.8	1.2
	96	46.6	104	58.1	14.7	2.8	3
NTP + MnO_2	48	67.6	36	87.5	2.9	1.4	1.4
	96	87.9	55	82.2	2.9	5.3	4.9

The chemical activity of ozone-promoted Al_2O_3–MnO_2 catalysis was also investigated. The catalyst was first saturated with isopropyl alcohol. Then, during the experiment, a known concentration of C_3H_7OH (500 and 160 ppm) was injected in an air stream between the corona reactor and the fixed-bed reactor. The amount of ozone in the air flow was varied from 150 to 600 ppm. The results, shown in Fig. 17, confirm that ozone-activated Al_2O_3–MnO_2 catalyst is very efficient for the destruction of C_3H_7OH. A complete removal of 160 ppm of C_3H_7OH is reached when adding 500 ppm of O_3. Isopropyl alcohol is almost completely oxidized in C_3H_6O, whose formation yield is around 95%. Only a few ppm of CO and CO_2 were detected. Acetone is much harder to decompose than isopropyl alcohol and is easily desorbed by the catalyst while feeding the fixed-bed reactor with isopropyl alcohol. For $[C_3H_7OH]_{initial}$ = 160 ppm, acetone concentration slightly diminishes for O_3 concentrations higher than 500 ppm. When almost all isopropyl alcohol has been removed, C_3H_6O starts to be oxidized on the catalytic sites, and the formation yield of CO_2 reaches about 10%. Residual ozone decreases when increasing C_3H_7OH initial concentration. Moreover, higher residual O_3 concentrations were measured when isopropyl alcohol injection was stopped at the end of the experiment. Therefore the capability of the catalyst to decompose ozone does not only depend on deactivation phenomena by CO_2, but also on the presence of adsorbed VOCs in the fixed-bed.

In order to achieve a better oxidation and to decompose the by-products, isopropyl alcohol was immobilized on the catalyst before the ozone-promoted treatment. The ozone concentration in the air stream was kept at 550 ppm in the course of the experiment. The temporal evolution of the effluent composition is shown in Fig. 18. In the first minutes, production of acetone (up to 130 ppm) was observed. C_3H_6O concentration is then quickly decreased after 50 min, while a significant amount of CO_2 is formed (more than 50 ppm). In the first phase of the treatment, immobilized isopropyl alcohol molecules are converted into acetone, which is partially released in the gas phase. The production of CO_2 increases gradually and remains above 50 ppm for several hours. This profile is due to the decomposition of more resistant organic compounds, probably the part of acetone that remains adsorbed on the catalytic sites. It is noteworthy that residual ozone concentration is continuously increased during the degradation of immobilized C_3H_7OH, which is in accordance with previous observations. In the course of the experiment, the amount of adsorbed organic

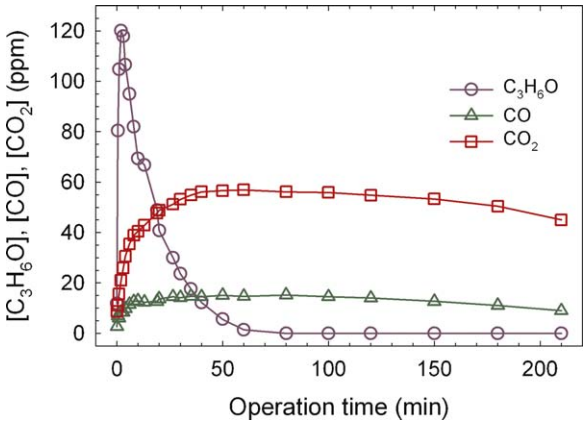

Fig. 18. Formation of by-products and O_3 decomposition during ozone-promoted destruction of immobilized isopropyl alcohol on Al_2O_3–MnO_2 catalyst ($[O_3]_{inlet}$ = 550 ppm).

compounds diminishes while produced CO_2 poison the catalytic sites, so ozone is less efficiently decomposed.

5. Conclusion

A pulsed corona discharges reactor serially combined with Al_2O_3–MnO_2 fixed-bed catalytic post-treatment has been tested for the treatment of dry air streams contaminated with two different VOCs (propane and isopropyl alcohol) at room temperature. The process was seen to improve the performance of non-thermal plasma for propane removal:

- The large amounts of ozone produced in the discharge reactor are efficiently decomposed at room temperature on Al_2O_3–MnO_2.
- Hazardous by-products (e.g. formaldehyde or methyl nitrate) resulting from the non-thermal plasma degradation of VOCs in NTP can be partially or totally removed.
- Higher destruction rates of the VOCs are obtained.
- The conversion of pollutant into CO_2 is favored over CO.

Ozone decomposition on MnO_2 sites leads to the formation of atomic oxygen which reacts with residual pollutants in the effluent after non-thermal plasma treatment. Therefore the catalytic post-treatment plays two major roles: to produce additional reactive species without injecting more energy and to recover the energy wasted in the production of oxygen atoms that mainly recombine to form O_3 during the post-discharge phase. Catalytic post-treatment allows the energy cost of VOCs removal by NTP to be significantly reduced (by a factors 2–4).

However, concerning isopropyl alcohol removal, even though DRE is improved after catalytic post-treatment, the oxidation is not complete. The formation yield of acetone increases and the adsorption of organic by-products on the fixed-bed is still a serious problem for long operation times. Ozone-promoted cleaning of the catalyst seems to be a promising solution.

It has been shown that the decomposition efficiency of ozone depends on the concentration of VOCs in the gas phase. The degradation efficiency of VOCs on Al_2O_3–MnO_2 slightly decreases in the course of catalytic post-treatment.

Acknowledgement

This research was performed in the frame of GDR CNRS 2495 "Cataplasme" (www.cataplasme.fr).

References

[1] B.M. Penetrante, M.C. Hsiao, J.N. Bardsley, B.T. Merritt, G.E. Vogtlin, A. Kuthi, C.P. Burkhart, J.R. Bayless, Plasma Sources Sci. Technol. 6 (1997) 251.
[2] M.G. Sobacchi, A.V. Saveliev, A.A. Fridman, A.F. Gutsol, L.A. Kennedy, Plasma Chem. Plasma Process. 23 (2003) 347.
[3] J. Jarrige, P. Vervisch, Plasma Chem. Plasma Process. 27 (2007) 241.
[4] E. Marotta, A. Callea, X. Ren, M. Rea, C. Paradisi, Int. J. Plasma Environ. Sci. Technol. 1 (2007) 39.
[5] U. Kogelschatz, Plasma Chem. Plasma Process. 23 (2003) 1.
[6] Y.S. Mok, C.M. Nam, M.H. Cho, IEEE Trans. Plasma Sci. 30 (2002) 408.
[7] L.A. Rosocha, R.A. Korzekwa, J. Adv. Oxid. Technol. 4 (1999) 247.
[8] J. Van Durme, J. Dewulf, W. Sysmans, C. Leys, H. Van Langenhove, Chemosphere 68 (2007) 1821.
[9] T. Oda, R. Yamashita, I. Hagai, T. Takahashi, S. Masuda, IEEE Trans. Ind. Appl. 32 (1996) 118.
[10] L. Magne, S. Pasquiers, V. Edon, S. Jorand, C. Postel, J. Amorim, J. Phys. D: Appl. Phys. 38 (2005) 3446.
[11] H.M. Lee, M.B. Chang, Plasma Chem. Plasma Process. 21 (2001) 329.
[12] R.G. Tonkyn, S.E. Barlow, T.M. Orlando, J. Appl. Phys. 80 (1996) 4877.
[13] T. Oda, A. Kumada, K. Tanaka, T. Takahashi, S. Masuda, J. Electrostat. 35 (1995) 93.
[14] R. Rudolph, K.P. Francke, H. Miessner, Plasma Chem. Plasma Process. 22 (2002) 401.
[15] H.H. Kim, Plasma Process. Polym. 1 (2004) 91.
[16] C. Ayrault, J. Barrault, N. Blin-Simiand, F. Jorand, S. Pasquiers, A. Rousseau, J.M. Tatibouet, Catal. Today 89 (2004) 75.
[17] M. Magureanu, N.B. Mandache, V.I. Parvulescu, C. Subrahmanyam, A. Renken, L. Kiwi-Minsker, Appl. Catal. B: Environ. 74 (2007) 270.
[18] C. Subrahmanyam, A. Renken, L. Kiwi-Minsker, Plasma Chem. Plasma Process. 27 (2007) 13.
[19] F. Holzer, U. Roland, F.D. Kopinke, Appl. Catal. B: Environ. 38 (2002) 163.
[20] U. Roland, F. Holzer, F.D. Kopinke, Appl. Catal. B: Environ. 58 (2005) 217.
[21] S. Futamura, A. Zhang, H. Einaga, H. Kabashima, L.Y. Hwan, Catal. Today 89 (2004) 89.
[22] O. Guaitella, F. Thevenet, E. Puzenat, C. Guillard, A. Rousseau, Appl. Catal. B: Environ. 89 (2008) 296.
[23] A.S. Besov, A.V. Vorontsov, Plasma Chem. Plasma Process. 27 (2007) 624.
[24] H.H. Kim, A. Ogata, S. Futamura, Appl. Catal. B: Environ. 79 (2008) 356.
[25] K.P. Francke, H. Miessner, R. Rudolph, Plasma Chem. Plasma Process. 20 (2000) 393.
[26] V. Demidiouk, J.O. Chae, IEEE Trans. Plasma Sci. 33 (2005) 157.
[27] R. Marques, S. Da Costa, P. Da Costa, Appl. Catal. B: Environ. 82 (2008) 50.
[28] M. Magureanu, N.B. Mandache, P. Eloy, E.M. Gaigneaux, V.I. Parvulescu, Appl. Catal. B: Environ. 61 (2005) 12.
[29] S. Futamura, A. Zhang, H. Einaga, H. Kabashima, Catal. Today 72 (2002) 259.
[30] S. Delagrange, L. Pinard, J.M. Tatibouet, Appl. Catal. B: Environ. 68 (2006) 92.
[31] S.B. Han, T. Oda, Plasma Sources Sci. Technol. 16 (2007) 413.
[32] J. Jarrige, P. Vervisch, J. Appl. Phys. 99 (2006), doi:10.1063/1.2202700.